JOINT EUROPEAN TORUS

JET–P(91)61

M. Bures, D. Campbell, N. Gottardi, J. Jacquinot, M. Mattioli, P. Morgan,
D Pasini, D.F.H. Start and JET Team

Low Particle Confinement H-Mode Observed during ICRF Heating on JET

Low Particle Confinement H-Mode Observed during ICRF Heating on JET

M. Bures, D. Campbell, N. Gottardi, J. Jacquinot, M. Mattioli[1], P. Morgan, D Pasini, D.F.H. Start and JET Team*

JET-Joint Undertaking, Culham Science Centre, OX14 3DB, Abingdon, UK

** See Appendix 1*

Preprint of Paper to be submitted for publication in
Nuclear Fusion

Low Particle Confinement H–mode observed during ICRF Heating on JET.

M.Bureš, D.Campbell, N.Gottardi, J.Jacquinot, M.Mattioli*,
P.Morgan, D.Pasini and D.F.H.Start.

JET Joint Undertaking, Abingdon, Oxon, OX14 3EA, UK
*EURATOM–CEA Association Cadarache, France.

Abstract.

During the H–mode experiments with ICRF heating on JET it was observed that the influxes of deuterium and impurities can substantially modify the quality of both the energy and particle confinement. In particular a **Low Particle Confinement(LPC) H–mode** was triggered either by deuterium input into the X–point region or as a result of a moderate impurity influx into the plasma boundary. In the LPCH–mode the particle confinement is at least 3 times less than in a normal H–mode. The energy, on the other hand, decreased by only ≈ 20%. The electron density, the deuterium density and the radiated power are also less than in a normal H–mode. However the deuterium dilution reaches a steady–state. The H–mode duration is extended by the LPC–phase to 2.8s and is limited only by the length of the heating pulse. The LPCH–mode particle confinement is linked to L–mode like particle diffusion within the radius $0.5<r/a<<0.8$ and the H–mode like barrier due to large V/D in the plasma boundary. This mode has the potential for substantially extending the H–mode phase to make it more reactor relevant.

1.0 Introduction.

The High Confinement Mode, in a tokamak with magnetic divertor, was first observed in ASDEX[1]. Since then the H–mode has been obtained on a large number of

tokamaks and with a variety of heating schemes[2–11]. Initially, on JET, H–modes were observed only with the Neutral Beam Injection(NBI) heating. Introduction of beryllium in JET[12] and the subsequent reduction of the "RF specific" impurity influxes from the Faraday screens of RF antennae[13,14] allowed H–modes with combined NBI+ICRF heating and also with the ICRF heating alone to be obtained. As reported earlier[15,16] the confinement properties of RF H–modes were comparable to those of NBI H–modes. Typically, the global energy confinement time was twice that given by Goldston scaling[17] and the local transport analysis indicated that the improvement occurred mainly in the outer plasma region bounded by the flux surfaces within $0.5 < \rho < 1$. In addition, the particle and impurity confinement was significantly enhanced and the density, radiated power and impurity concentration generally increased throughout the H–mode. Termination of the H–mode was attributed to the radiated power reaching $\approx$ 60% of the input power.

In this paper we describe some of the results from the latest series of JET H–mode experiments with ICRF heating alone. In particular a new regime is discussed in which **the particle confinement is substantially reduced while the discharge continues to benefit from the high confinement of energy**. The successful operation of the next step device will require a high energy and low particle confinement scenario and at present it is suggested that the Edge Localised Modes(ELMs) will provide the control of particle and impurity confinement. The Low Particle Confinement H–mode appears to be triggered by enhanced radiation from the outer region, $r/a > 0.5$, of the plasma and is characterised as ELM–free because the typical D_α bursts, usually associated with ELMs, are absent. In the experiments described below, the LPCH–mode was achieved either by deuterium puff into the X–point region or by injection of nickel trace impurity into the plasma boundary. Modification of both energy and particle confinement was also observed when deuterium pellets of 2.7 mm diameter, which have shallow penetration depth, were injected into the boundary of the H–mode discharge.

2.0 Experimental arrangements.

The JET device is a low aspect ratio tokamak with major radius R_0= 2.96 m and minor radius a=1.2 m. In the series of experiments reported in this paper the plasma was operated in a Double Null X–point(DNX) configuration with the toroidal field on axis B_0=2.8 T, plasma current I_p=3 MA and elongation $\kappa \approx 1.8$. Direction of the toroidal field and the details of the magnetic configuration were such that the power flowing in the Scrape–off–Layer(SOL) was interacting with the carbon protection tiles at the upper X–point(the ion ∇B – drift towards this dominant X–point). The low field side RF antennae were fitted with new beryllium Faraday screens which replaced the old water cooled nickel screens. The heating scheme used a hydrogen minority in a deuterium plasma(D(H) scenario) and the majority of discharges utilized the toroidal dipole $(0,\pi)$ phasing of the antennas with k_{II}= 7m^{-1}. The frequency was adjusted so that the minority cyclotron resonance passed through the magnetic axis.

Changes of the edge parameters during the H–mode modify the propagation of the RF wave and result in a rapidly changing load to the RF generators. It is then difficult to sustain a high power input at a constant level. A new feature of these experiments involved control of the plasma position by a feedback loop acting on the value of the coupling resistance R_c. Consequently a constant value of R_c was maintained during both the L and H phases. This permitted improved tuning and, as a result, the RF power could be maintained at a constant level. During the experiments, described in this paper, the power did not exceed P_{RF}= 10 MW. This limit was imposed by the carbon influxes from the x–point target plates.

3.0 Low particle confinement H–mode.

3.1.LPCH–mode induced by gas input into the x–point.

As we discussed briefly in the Introduction the ICRF heated H–modes are sensitive to the influxes such as RF specific influxes from the antennae screens or the controlled influxes by gas puffing, edge pellet fuelling or nickel trace injection. The entire ICRF H–mode data base is plotted in Fig.1, where the plasma energy content, measured by the diamagnetic loop, is compared to the Goldston scaling. At first sight, the data set exhibits a large scatter. The best H–modes, in terms of the energy confinement, are those where the discharge evolved without any additional particle input(deliberate or accidental) into the plasma boundary. Typically, these would reach energy content $W \geq 2.5\ W_G$. The fraction of energy stored in the fast ions is in the range $0.05<W_f/W_{dia}<0.15$. The rest of discharges, with the pellets, nickel, carbon fragment or gas introduced into the boundary, have somewhat reduced confinement. The systematically lower confinement with monopole phasing is consistent with existence of the convective cell[18,19] in front of the Faraday screen which interacts with the H–mode boundary barrier.

Two examples of a modified H–mode(LPCH), which has not been previously observed on JET, are pointed out in Fig.1. The first example was obtained by gas puffing into the X–point region(but outside the volume defined by the separatrix and the x–point). Gas introduction started before the application of ICRF–heating power and was sustained during the entire H and LPCH–phases. The traces of the radiated power, D_α light, plasma stored energy and ICRF power are plotted in Fig.2. The onset of H–mode takes place at t≈12s and the first phase of the H–mode untill t≈13.6s can be characterised as a regular H–mode. However there is one important difference. In a regular H–mode the gas input from the valve is usually automatically switched–off when the density starts to rise after the L–>H transition. In this case a forced gas influx ϕ_g of the order of 3–5 x 10^{21} deuterons s^{-1} was maintained throughout the entire H–mode phase. Correspondingly the radiated power is substantially higher than in a regular H–mode[15,16,20] by factor 2 to 3. When the total radiated power,

including power from the X–point region, reaches ≈10 MW and the power flowing into the plasma edge $P_{EDGE}= P_{\Omega}+ P_{RF}-dW/dt-P_{RAD}^{BULK}$ drops from ≈5.3 to ≈4 MW a sudden "switch" in the particle confinement is seen in the trace of P_{RAD} in Fig.2 and in the trace of $N_e= <n_e>V$ in Fig.3($<n_e>$ is the volume averaged plasma density and V is the plasma volume). The evolution of the plasma energy content shows a reduction already before the the H –> LPCH transition due to a dramatically increasing radiated power. The maximum energy content, reached during the discharge at t≈13 s, is 2 x W_G which then drops by ≈ 15–20 % during the LPCH phase. Note that the LPCH–>L transition takes place during the ramp–down of RF power. The H–mode termination by the radiation spike in the X–point region, which is the usual cause of H–mode termination, was delayed and the duration of the LPCH–mode could have been extended for a longer period by continuing the RF heating. The energy evolution during the LPCH–mode has a finite positive slope which might be due to gradual improvement in the confinement. That might be important if the steady–state could be achieved. There is no doubt that the steady–state for impurity concentration was already obtained in this discharge. During the LPCH–phase the deuteron dilution remained constant at the level n_D/n_e ≈0.65 as indicated by constant Z_{eff}. To reach the steady–state in density could be achieved by the simultaneous increase of gas puff and RF power.

To calculate the change in the global particle confinement time is possible only if both the deuterium and impurity influxes are measured quantitatively. This is not done in the experiments. However the confinement of deuterium can be estimated with a reasonable accuracy. The global impurity behaviour is well described by the evolution of Z_{eff}, plotted in Fig.3. Assuming that the principal impurity is carbon, the total number of deuterons N_D can be calculated(see Fig.3). The characteristic confinement time of deuterons can be now derived from the N_D evolution and the gas input from the valve ϕ_g in form

$$\tau_p^*= N_D/(\phi_g - dN_D/dt)$$

which can also be defined as

$$\tau_p^* = \tau_p/(1-R_D)$$

Here $R_D = \phi_R/(N_D/\tau_p)$is the deuterium recycling coefficient, τ_p is the particle confinement time defined at the plasma edge and the ϕ_R is the deuteron recycling flux. Given the values N_D, ϕ_g and $\delta(dN_D/dt)$ at t ≈ 13.6s(H–>LPCH transition) the change of τ_p^* can be estimated. In particular, τ_p^* decreases from ≈1.5 to ≈0.5s. Assuming that the deterium recycling does not change significantly during the transition the factor ≈3 change in τ_p^* represents the change in τ_p. Given the method used to derive τ_p^* and the error bars in the data, in particular the gas input ϕ_g and $\delta(dN_D/dt)$, the absolute value of this parameter should be taken with care. It represents only a rough measure of the τ_p change. Despite this uncertainty it can be stated that the particle confinement time changes by a large factor while the confinement of energy is reduced at most by ≈ 20% as indicated in Fig.2. The confinement of impurities will be discussed in Section 3.4 for another example of the LPCH–mode.

The features of the LPCH–mode, induced by the strong gas puff, are i)slightly enhanced recycling both at the wall(D_α^{Wall} signal in Fig.2) and X–point region(D_α^{XPT} signal in Fig.4), ii)slightly relaxed density gradient at the plasma edge. The latter can be deduced from measurements of the plasma–antenna distance, in Fig.4 denoted d_{a-p}. At the switch of τ_p at t ≈ 13.6 s, the plasma position feedback system increases the separation d_{a-p} in order to maintain constant RF coupling resistance R_c. In other words, the same coupling resistance at larger antenna–plasma distance implies a relaxed density gradient in front of the Faraday screen. With respect to MHD activity it is found that the transition is not associated with low m,n (< 3) MHD modes as no correlation with such modes could be found.

3.2. Features of energy transport in the gas–puff induced LPCH–mode.

The mechanism for the H–>LPCH transition is not understood. Nevertheless it can be concluded that the transition is a result of strongly modified energy balance in the outer region of the plasma. The strong gas puff induces additional density rise and, in particular, a corresponding increased radiation loss coming predominantly from the r/a>0.5 region(Fig.11). To support this thesis two regular H–modes(cases a,b) are compared to the gas–puff case c in Fig.5. The regular H–modes were obtained at somewhat different level of input power and the duration of these H–modes is relatively short.(The H–>L transition is triggered by a radiation spike from the X–point region. It is a similar spike as the one which is associated with the LPCH–>L transition seen in Fig.2) First we note the behaviour of radiated power(radiation from the x–point region excluded) which, in the gas–puff case, is substantially enhanced. The resulting edge electron temperature, measured by the fast ECE system, is at least factor 2 lower than in the regular H–mode. The T_e error bar is ± 10% in absolute value and ±5cm in radial position. In Fig.6 the edge temperatures are plotted against the plasma radius. The "profile" denoted by dots refers to the time of the H–>LPCH transition. The remaining profiles are plotted at the times when the T_e^{EDGE} is maximum. Position of the Last Closed Magnetic Surface(LCMS) is defined by the MHD equilibrium code using the magnetic data. Within the error bars the two outermost channels can be taken as indicative of the T_e pedestal. The role of the energy balance in the outer plasma region is further strengthened by the qualitative correlation of the time evolution of T_e and P_{EDGE}(see Figs.5 and 6). In all regular H–modes the P_{EDGE} and T_e increase monotonically untill the time when the transition H–>L occurs. In the H–mode with the strong gas puff the P_{EDGE} first reaches a maximum (t≈13s) and then starts to decay. Subsequently the H–>LPCH transition is triggered at t≈13.6s. In the regular H–mode the H–>L transition occurs when P_{EDGE} reaches ≈6.5 MW and the H–>LPCH transition in the gas–puff case takes place when P_{EDGE} droppes to ≈4.5 MW. Note that the transitions does not occur in the same time.

As discussed in the previous Section the global energy confinement during the LPCH–mode is degraded only marginally. Thus we expect that the local transport is similar to that in a regular H–mode. In the H–mode the improved confinement occurs primarily in the outer plasma regions, i.e., at $r/a \geq 0.5$. To estimate the values of the thermal conductivity at the H–>LPCH transition we adopt the cylindrical model of Callen et al.[21] and assume that $T_e \approx T_i$ and that the plasma is in equlibrium. The ion temperature profiles were not measured, however, the central electron and ion temperatures were, within the error bars, equal. This is not surprising because the plasma density was high and so was the minority concentration. Thus the proton minority tail is expected to be below or close to the critical energy for electron respectively ion heating. This is confirmed by the estimate of the fraction of the fast ion energy $W_f/W_{dia}=2(1- W_{kin}/W_{dia})/3$. It is less than 10% in the H–phase and $W_f/W_{dia} \approx 0$ at the time of the H–>LPCH transition. The central temperatures are plotted in Fig.4. We note that the ion temperature deduced from neutrons(broken line) is during the first second overestimated. This is attributed to presence of the $2\omega_{CD}$ tail which disappears with the rising density. Further we consider region 3.6 <R <4.0 m, where the convective losses are assumed to be negligible compared to the diffusive loss. Thus the integration of the energy balance yields the diffusive heat flux

$$-n(r)\,\chi_{eff}(r)\,A(r)\,\frac{dT(r)}{dr} = P_{\Omega}(r) + P_{RF}(r) - P_{RAD}(r)$$

in which $A(r) = 4\,\pi^2\,R_o r$. Power inputs P_{Ω}, P_{RF} and the radiated power $P_{RAD}(r)$ within the volume $V(r)=2\pi^2 R_o r^2$ are

$$P_i(r) = 4\,\pi^2\,R_o \int_0^r r'\,p_i(r')\,dr', \qquad i = \Omega, RF, RAD.$$

The volume V(r) is defined by the magnetic flux surface of area A(r) and R_0 is the major radius. The RF power deposition was calculated using the ray tracing code FREMIR[22] and, as usual, the deposition profiles are peaked. Typically ≈90% of power is absorbed within $r/a \leq 0.45$. The average χ_{eff} is $\approx 2 \pm 1$ $m^2 s^{-1}$ but is slightly higher at the inner radius R=3.6 m and slightly lower at the outer radius R=4m. It can be concluded that the derived values are in the range previously derived[16] for the H–modes with the energy confinement twice that of Goldston.

3.3. LPCH–mode induced by nickel injection.

The second clear example of the LPCH–mode was obtained with the nickel injection and is plotted in Figs.7a and 7b. In this case the amount of injected nickel(usually injected in a small amount to study the nickel transport) is not negligible and the corresponding radiated power increase reaches $\delta(P_{RAD}^{TOT}) \approx 4$ MW, with 1 MW radiated from the X–point region. At the same time a sudden drop in the particle confinement τ_p is induced. As a result the bulk radiated power then decreases throughout the remainder of H–mode due to the decreasing plasma density(Fig.8) while the power radiated in the x–point remains constant. In Figs.7 and 8 the LPCH–mode is shown to last for ≈ 1s. During the LPCH–phase the plasma density $<n_e> = N_e/V$ decays, as opposed to the density rise always observed during the H–phase. The deuterium density also decays, and somewhat faster than the electron density, because the yield of main impurity, carbon, is higer than one and the deuterium input from the gas valve is zero. As can be seen from results presented in the previous Section a strong deuterium puff during this phase could bring the deuterium dilution into steady–state.

The change in the global particle confinement time during H–>LPCH transition can be estimated in an identical way as in Section 3.1. Because the gas input ϕ_g=0 at t > 12.6s the change $\delta(dN_D/dt)$ at the time of H–>LPCH transition(≈ 13s) is a direct measure of the change in τ_p^*. Thus τ_p^* decreases from ≈5 to ≈1s. Assuming that τ_p is comparable to the confinement of impurities, derived below, the recycling of deuterium R_D has to be significantly below one. We note that the values τ_p^* are higher than in the case with gas puffing. However, in both cases a significant τ_p^* reduction is observed.

As in the previous case with gas puff the energy balance in the outer plasma region is significantly modified by the enhanced radiation due to the injected nickel. In this case the P_{EDGE} is transiently(≈150 ms) decreased from ≈4.5 MW to ≈1.5MW which is sufficient to trigger the H–>LPCH transition. The amount of injected nickel are a few 10^{18} ions. The increase of bulk radiation allows an estimation of the average nickel radiation constant $<L^{Ni}>$ characteristic of the H–mode. It is as defined,

$P_{RAD}^{Ni} = <n_e><n_{Ni}><L^{Ni}>V$ and is typically $<L^{Ni}> \approx 2–3 \times 10^{-32}[Wm^3]$.

3.4. Laser–injected nickel behaviour.

An objective of injecting a small quantity of nickel impurity by laser ablation into the plasma is to investigate the transport of impurities. In the discharge described above the amount was sufficient to trigger the H–>LPCH transition. The intensity of the NiXXV line(117.94 Å) normalised to the line averaged density is plotted in Fig.9. It represents a measure of the number of nickel ions along the line of sight. Correction due to the temperature variation is small. The characteristic decay times of such signals are representative of the impurity confinement times. The ratio of the decay times in H and L–modes is ≈10, indicating that the impurity confinement in H–mode is increased by an order of magnitude. This large increase in τ_{imp} is always observed, in both the ICRF and NBI–heated H–modes[23, 24]. In contrast, during the LPCH–mode, τ_{Ni} has an intermediate value ≈1s. The factor ≈3 reduction, with respect to the H–mode, is consistent with the τ_p^* reduction discussed in Sections 3.1 and 3.3.

The transport of impurities into the plasma following laser ablation was followed with good spatial and temporal resolution using two soft x–ray cameras together with VUV and x–ray spectrometers. The experimental data, namely, the absolute x–ray emissivity profiles and the spectroscopic line brightnesses time evolution were then simulated using an impurity transport code. In the code the impurity flux for each ionization stage is described by an expression of the type

$$\Gamma_z(r) = -D(r)\,(\partial n_z/\partial r) - V(r)n_z\,.$$

The best match between the simulation and the experimental data then provides a measurement of D(r) and V(r).

The impurity transport parameters thus obtained to simulate the impurity behaviour in the LPCH–mode discharge are shown in Fig.10. In the central region $\rho = r/a < 0.2$ the diffusion coefficient D is small and close to the neoclassical predictions.

This is a general feature also observed between sawteeth in ohmic and L–mode discharges and during regular H–mode discharges[23, 24]. Within the intermediate region $0.2<\rho<0.8$ the value of $D \approx 2.5 m^2 s^{-1}$ reaches roughly thirty times the neoclassical value and is characteristic of L–mode discharges. In regular H–mode plasmas, on the other hand, the typical values are factor 5–10 lower as indicated by the dashed region in Fig.10. The edge region, $\rho>0.9$, develops a transport barrier in usual fashion. The strong increase of the inward convection velocity in the narrow region inside the separatrix is needed to simulate the behaviour of both the intrinsic and laser ablated impurities in H–mode plasmas[24,25,26]. The shape of D(r) beyond $\rho=0.8$ is somewhat arbitrary as any selected value of D(within reasonable bounds) and the matching value of V can simulate the impurity data satisfactorilly. If we keep the value $D=2.5\ m^2 s^{-1}$ up to the plasma edge the resulting inward pinch velocity would have to be higher than the corresponding pinch velocity in a regular H–mode. To summarise the simulation of the LPCH–mode, it is characterised by the L–mode like diffusion coefficient $D_{LPCH}(0.5 \leq \rho \leq 0.8)) = 5–10 \times D_H$. Also the efficiency of the transport barrier, measured by the ratio V/D at the edge, is reduced by a factor ≈ 2 when compared to a regular H–mode.

4.0 Discussion.

The trigger mechanism for the LPCH–mode is not understood but it appears to be related to the energy balance in the outer region of the plasma where the enhaced radiation(in both cases of the gas–puff and nickel injection) takes place. The edge temperature is reduced due to the drop in the P_{EDGE} which can be induced either slowly by gas–puff or transiently by the nickel injection. The two types of discharges were run at different plasma densities, see Fig.11, and the transition took place at different edge electron temperatures. Thus it seems that the additional "hidden" parameter(s) in conjucton with the T_e^{edge} drop is/are responsible for the trigger. It is interesting to note that the electron pressure profile is similar in the two cases. The error bars on the electron temperature profiles as well as density profiles are ±10% in absolute value. Error bar of the central electron density value might be somewhat higher because one channel of the interferometer was missing. Error bar on the radiated power does not exceed ±15%.

A similar mode with high energy confinement and the density in a quasi–stationary state has been observed in JFT–2M[10]. In that mode the edge temperature is also lower than in the H–mode. However other aspects of the behaviour are somewhat different. In particular the energy confinement is higher than in a regular H–mode and is attributed to the density peaking. The radiation level increases in the core region. Another improved confinement mode, with central density peaking, was obtained with the counter NBI in ASDEX[11]. In this mode both the energy and particle confinement are enhanced in contrast to the degradation, mainly in τ_p, in the LPCH–mode.

5.0 Conclusions.

A major improvement of the JET ICRF–heating performance resulted from elimination of the "RF specific" impurity influxes by introducing beryllium Faraday screens. ICRF–heated H–modes with energy content above 2.5 x W_G can be now routinely achieved. The results presented in this paper demonstrate that the

confinement of ICRF–heated H–modes is sensitive to the gas and impurity influxes. A new regime **Low Particle Confinement H–mode**, which exhibits a strongly degraded particle and impurity confinement, was observed. Typically the regular H–mode particle confinement is $\tau_p^H \geq 3s$ while in the LPCH–mode it is lower, e.g., $\tau_p^{LPCH} \approx 1s$. The intermediate(between L and H) particle confinement is found to be linked to the L–mode–like particle diffusion in the bulk of the plasma and the H–mode like barrier of enhanced V/D at the plasma boundary. The energy confinement of the LPCH–mode is degraded only by ≈20%. To reach the steady–state in density was not attempted in the LPCH–phase but could be achieved by the simultaneous increase of gas input in conjuction with increased RF power. However the deuterium dilution reaches the steady–state. The LPCH–modes appear to be ELM–free in a sense that the usual D_α signature of ELMs is absent. The LPCH–mode has the potential for extending the regular H–mode phase to make it more reactor relevant. The low particle confinement is a necessary but not sufficient condition for the successful application of this mode. It is important that the impurity yield is low enough. The gas puff is one possible ingredient as indicated by the results presented here.

Acknowledgements.

We wish to thank our colleagues in the JET team, especially the tokamak operating teams and those operating the diagnostics used in the experiments reported in this paper.

References.

[1] WAGNER, F., BECKER, G., BEHRINGER, K., et al., Phys. Rev. Lett. 49(1982)1408.

[2] KAYE, S., BELL, M.G., BOL, K., et al., J.Nucl. Mater. 121(1984)115.

[2] SENGOKU, S., and JFT–2M Team, J. Nucl.Mater. 145–147 (1987)556.

[4] BURRELL, K.H., EJIMA, S., SCHISSEL, D.P., et al., Phys. Rev. Lett. 59(1987)1432.

[5] TANGA, A., BARTLETT, D.V., BEHRINGER, K., et al., Proc. 11th Int. Conf. on Plasma Phys. and Contr. Nucl. Fus. Res. Kyoto 1986, Vol.1,(IAEA, Vienna 1987)65.

[6] LOHR, J.M., STALLARD, B.W., PRATER, R., et. al., Phys. Rev. Lett. 60(1988)2630.

[7] HOSHINO, K., YAMAMOTO, T., SUZUKI, N., et al., Nucl. Fusion 28(1988)301.

[8] STEINMETZ, K., WAGNER, F., WESNER, F., et al., Contr. Fus. and Plasma Heating(Proc. 13th Eur. Conf. Schliersee, 1986)Vol.10C, Part II, Europ. Phys. Soc., p.21.

[9] MATSUMOTO, H., OGAWA, T., TAMAI. H., et al., Nucl. Fusion 27(1987)1181.

[10] MORI, M, SUZUKI, N., UESUGI, Y., et al., Nucl. Fus., Vol.28, No.10(1988)1892.

[11] GEHRE, O., GRUBER, O., MURMANN, D., et al., Phys. Rev. Lett., Vol.60, No.15(1988)1502.

[12] THOMAS, P.R. and The JET Team, J. Nucl. Mat. 176 & 177(1990)3.

[13] BUREŠ, M., JACQUINOT, J., LAWSON, K., et al., Plasma Phys. and Contr. Fus. Vol.33, No.8(1991)937.

[14] D'IPPOLITO, D., MYRA, J., BUREŠ, M. and JACQUINOT, J., Plasma Phys. and Contr. Fus. Vol.33, No.6(1991)607.

[15] TUBBING, B.J.D., JACQUINOT, J., STORK, D. and TANGA A., Nucl. Fusion, Vol.29, No.11(1989)1953.

[16] BHATNAGAR, V.P., JACQUINOT, J., TUBBING, B.J.D. et al., Plasma Phys. and Contr. Fus., Vol.33, No.2,(1991)99.

[17] GOLDSTON, R., Plasma Phys. and Contr. Fus. Vol.26(1984)87.

[18] The JET Team, presented by J.JACQUINOT, Invited paper 18th Eur. Conf. Berlin 1991, to appear in Plasma Phys. Contr. Fusion.

[19] D'IPPOLITO, D. A., MYRA, J.R., JACQUINOT, J. and BUREŠ, M., Proc. 9th Topical Conf. on RF Power in Plasmas, Charleston, August 1991.

[20] BHATNAGAR, V., BOSIA, G., BUREŠ, M. et al., Contr. Fus. and Plasma Heating(Proc. 18th Eur. Conf. Berlin, 1991) Vol. 15C, Part I, Europ. Phys. Soc., p.369.

[21] CALLEN, J.D., CHRISTIANSEN, J.P., CORDEY, J.G., et al. Nucl.Fusion, Vol.27, No.11(1987)1857.

[22] JACQUINOT, J., in Heating in Toroidal Plasmas(Proc. 1st Joint Varenna–Grenoble Int. Symp. Grenoble, 1978), Vol.1, Pergamon Press, New York(1979)127.

[23] PASINI, D., MATTIOLI, M., EDWARDS, A. et al., Nucl. Fusion, Vol.30, No.10(1990)2049.

[24] PASINI, D., DENNE–HINOV, B., GIANNELLA, R., et al., Contr. Fus. and Plasma Heating(Proc. 18th Eur. Conf. Berlin, 1991)Vol.15X, Part I, Europ. Phys. Soc., p.33.

[25] HAWKES, N., WANG, Z., BARNSLEY, R., et al., Contr. Fus. and Plasma Heating(Proc. 16th Eur. Conf. Venice, 1989)Vol.13B, Part I, Europ. Phys. Soc., p.79.

[26] GIANNELLA, R., BEHRINGER, K., DENNE, B., et al., Contr. Fus. and Plasma Heating(Proc. 16th Eur. Conf. Venice, 1989)Vol.13B, Part I, Europ. Phys. Soc., p.209.

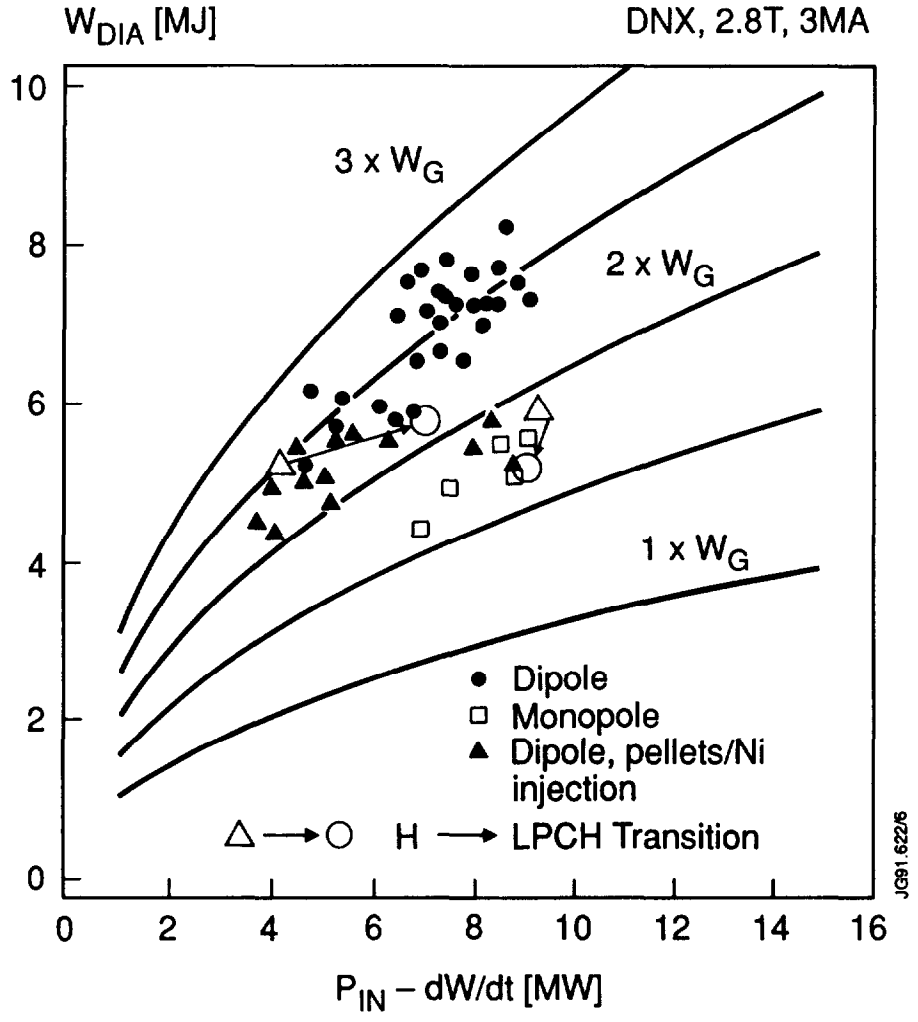

Fig.1 Plasma stored energy measured by the diamagnetic loop plotted as a function of the power loss from the plasma. The data are compared to 1, 1.5, 2, 2.5 and 3x values defined by the Goldston scaling $W_G=6.4x10^{-8}I_p(A)P^{1/2}(W)R^{1.75}(cm)a^{-0.37}(cm)\kappa^{1/2}$. 2 particular H–modes and their transition into the Low Particle Confinement H–modes are pointed out. Dipole refers to $k_{II}=7\ m^{-1}$ antenna phasing and monopole to $k_{II}=0\ m^{-1}$.

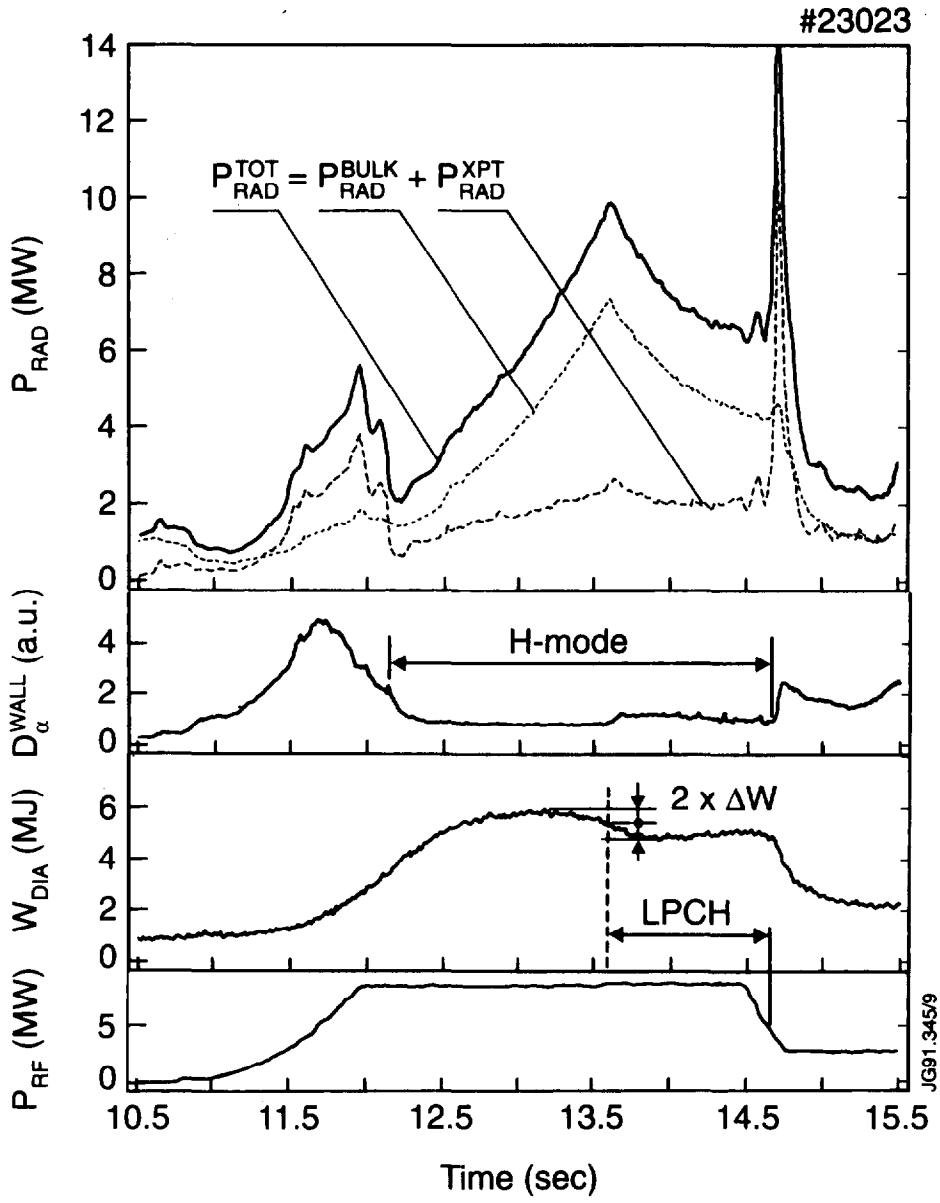

Fig.2 Radiated power, D_α at the vessel wall, plasma stored energy and RF power input during the RF heated X–point discharge #23023. The H–mode is indicated by the drop of D_α signal and the LPCH–mode is characterised by the P_{RAD} decay. A partial confinement degradation, before the H–>LPCH transition, is due to the high radiated power.

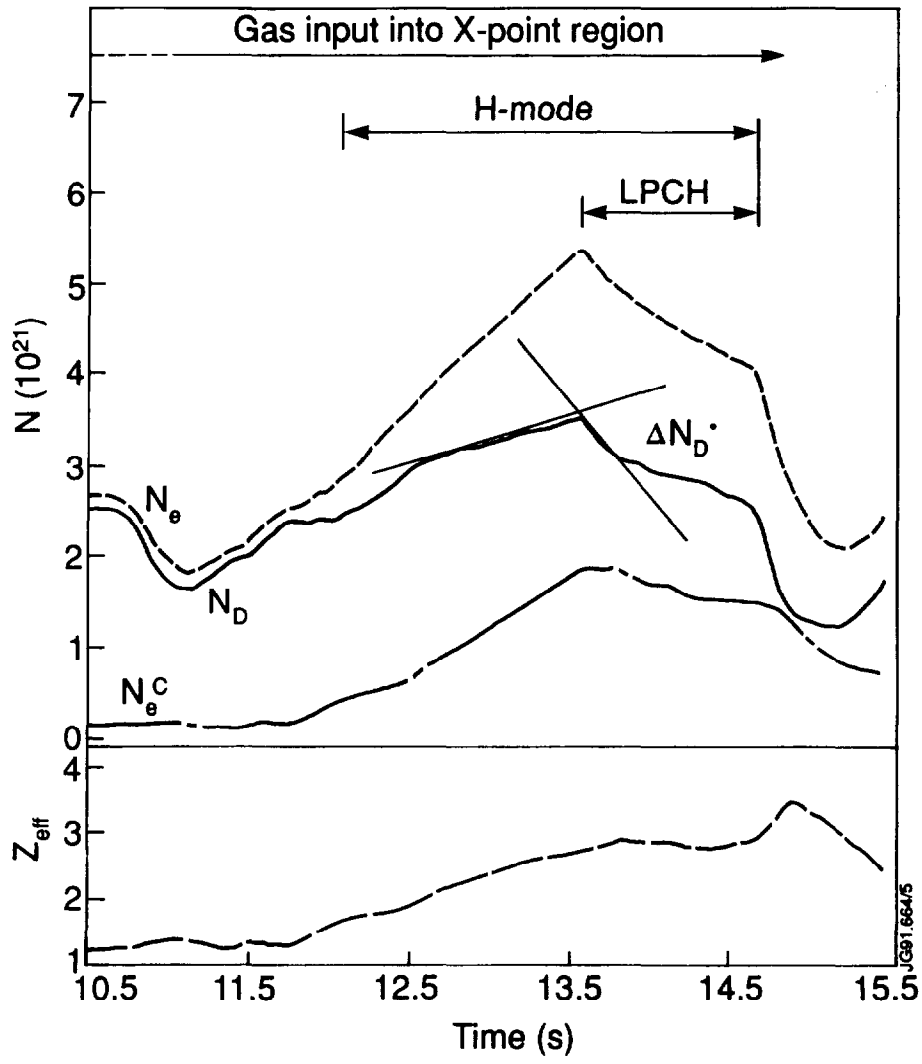

Fig.3 Evolution of the total number of electrons N_e, deuterons N_D, electrons due to carbon N_e^C in the plasma volume and Z_{eff}. The change of the derivatives at the H–>LPCH transition should be noted. During the LPCH the deuterium dilution remains constant($Z_{eff} \approx$ const.).

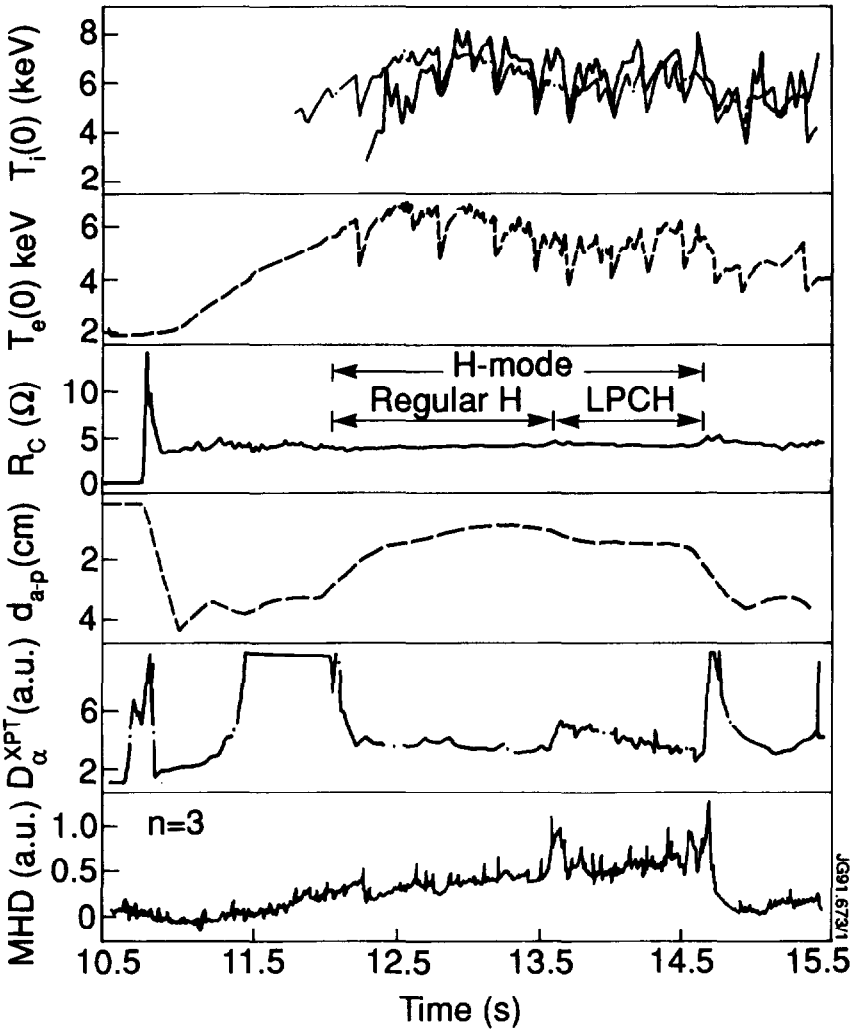

Fig.4 The central ion temperature measured by X–ray spectroscopy(broken line) and by neutron emission, central electron temperature(ECE), antenna–plasma coupling resistance, antenna–plasma distance, recycling D_α light from the x–point region and the MHD signal(n=3) measured at the plasma boundary.

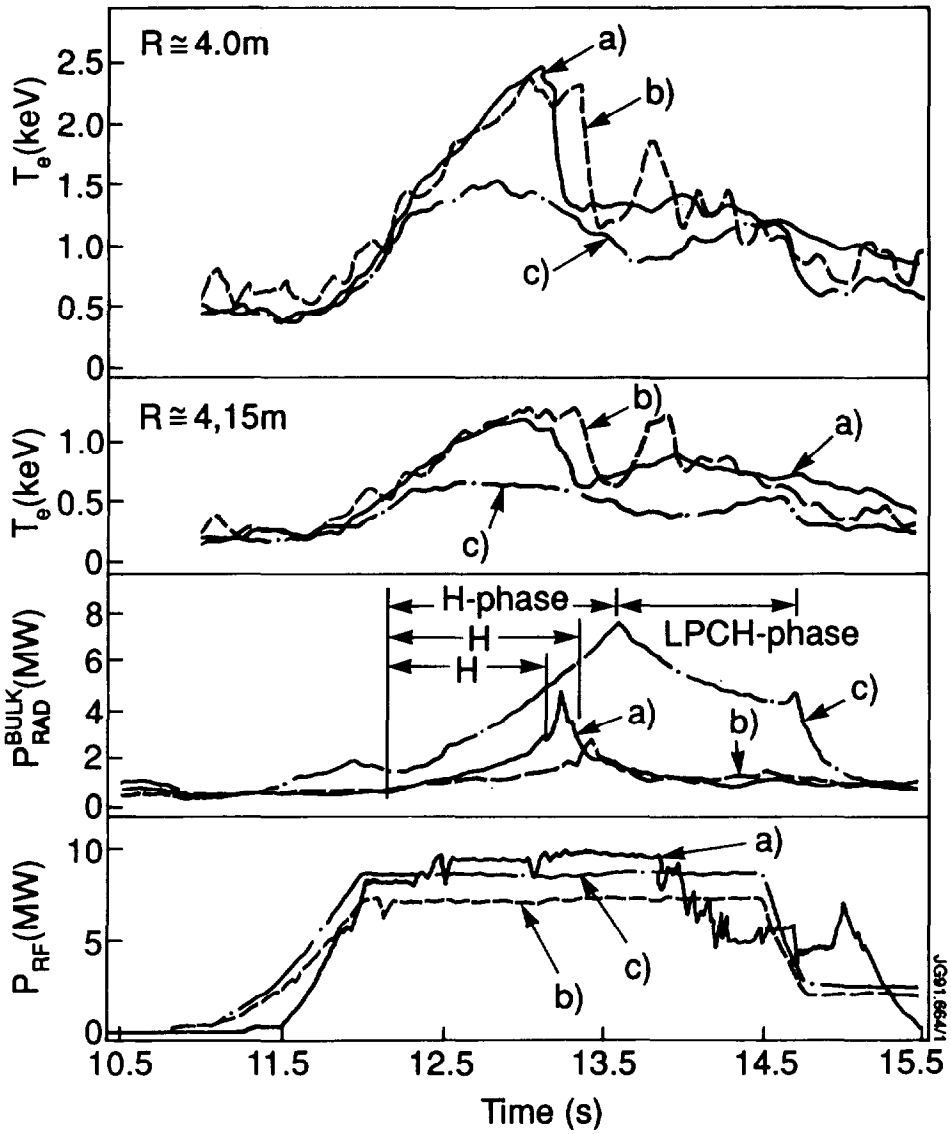

Fig.5 Comparison of two regular RF H–modes(a and b) with the H–mode modified by a strong gas puff(c). The input RF power, bulk radiated power and the edge electron temperature at two radii are shown.

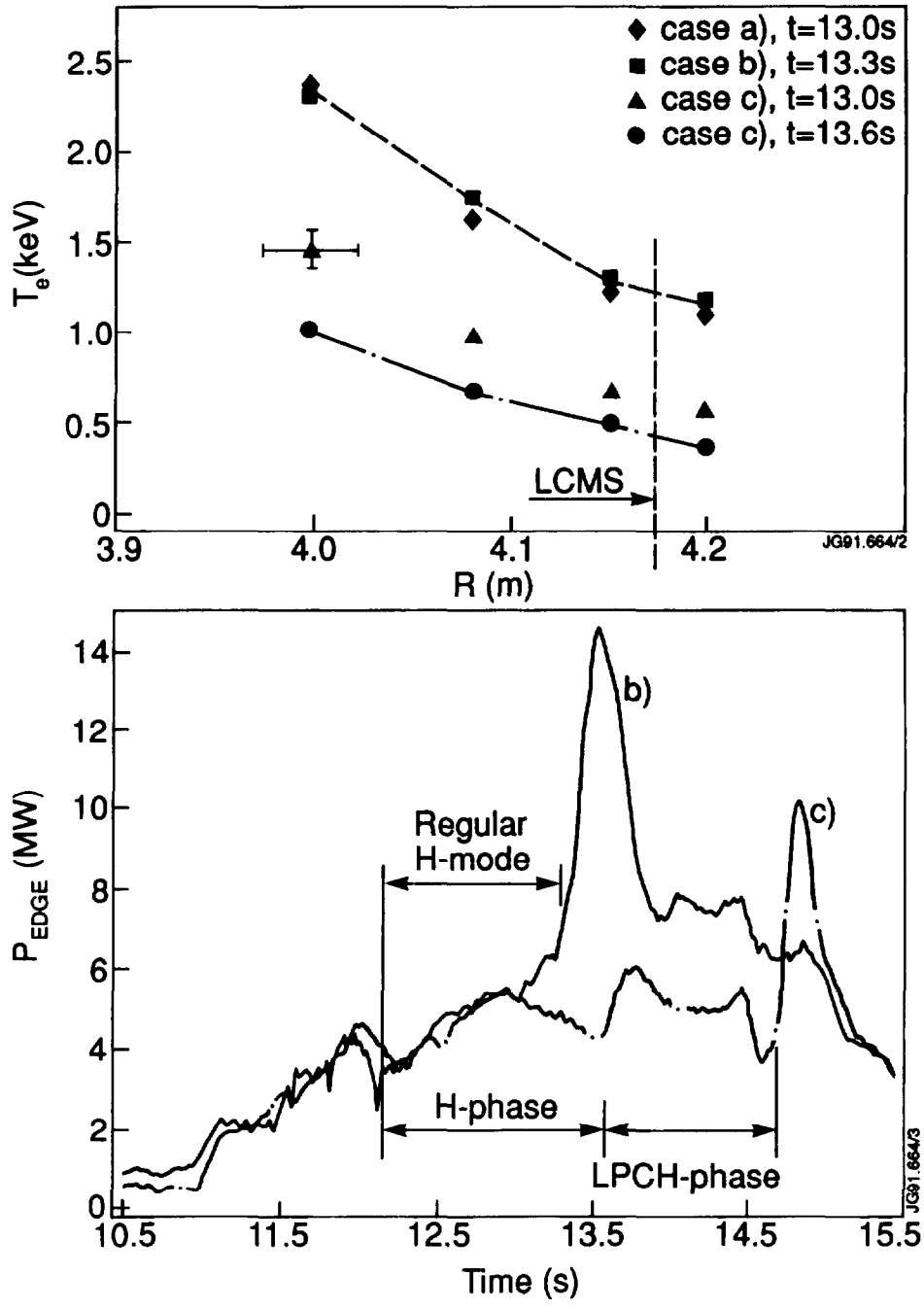

Fig.6 Edge electron temperature measured at four radii close to the LCMS for the same discharges as in Fig.5. The dots correspond to the T_e profile at the H–>LPCH transition. In the lower figure the time evolution of the P_{EDGE} in a regular H–mode is compared to the gas–puff case.

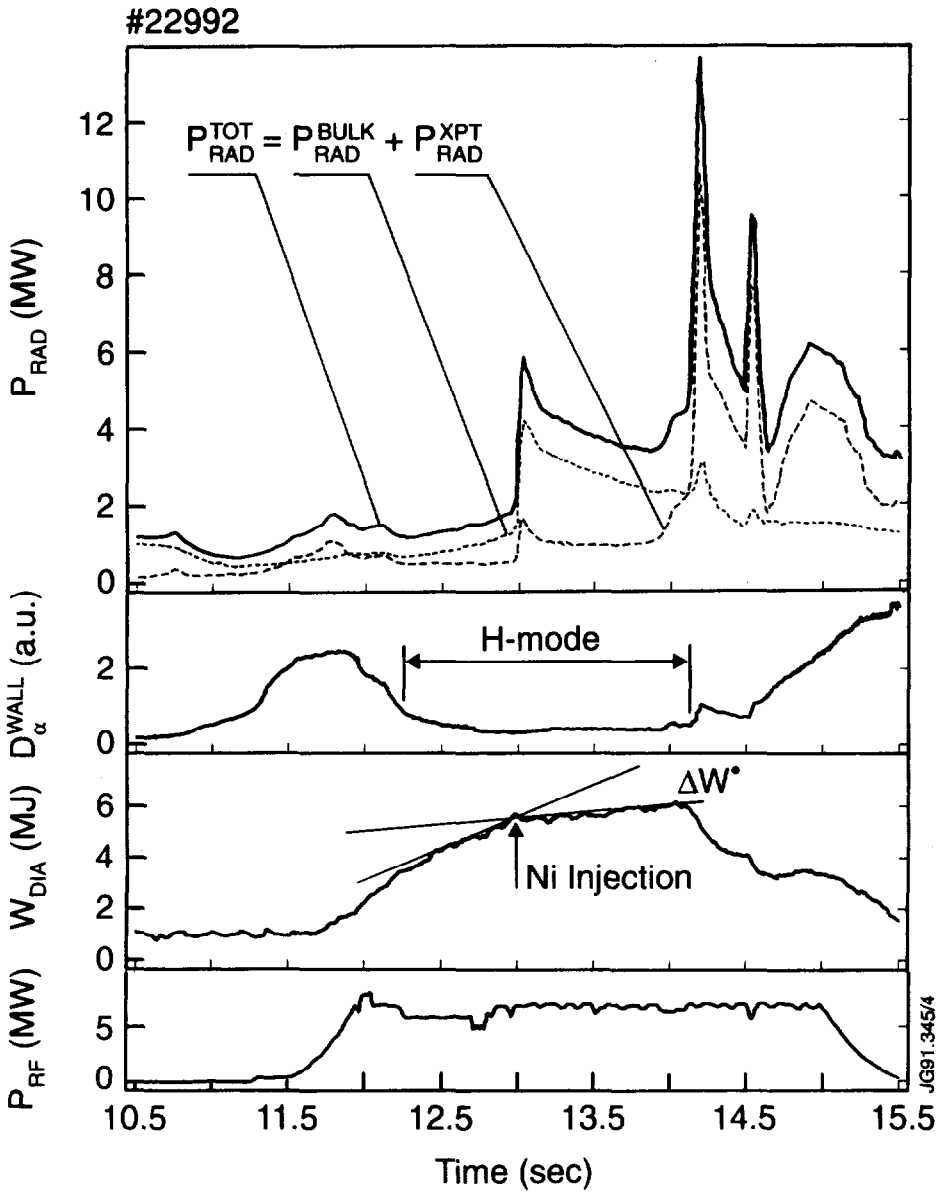

Fig.7a Radiated power, D_α at the vessel wall, plasma stored energy and RF power input during the RF heated X–point discharge #22992. The H–mode is indicated by the drop of D_α signal while the LPCH–mode is characterised by the P_{RAD} decay.

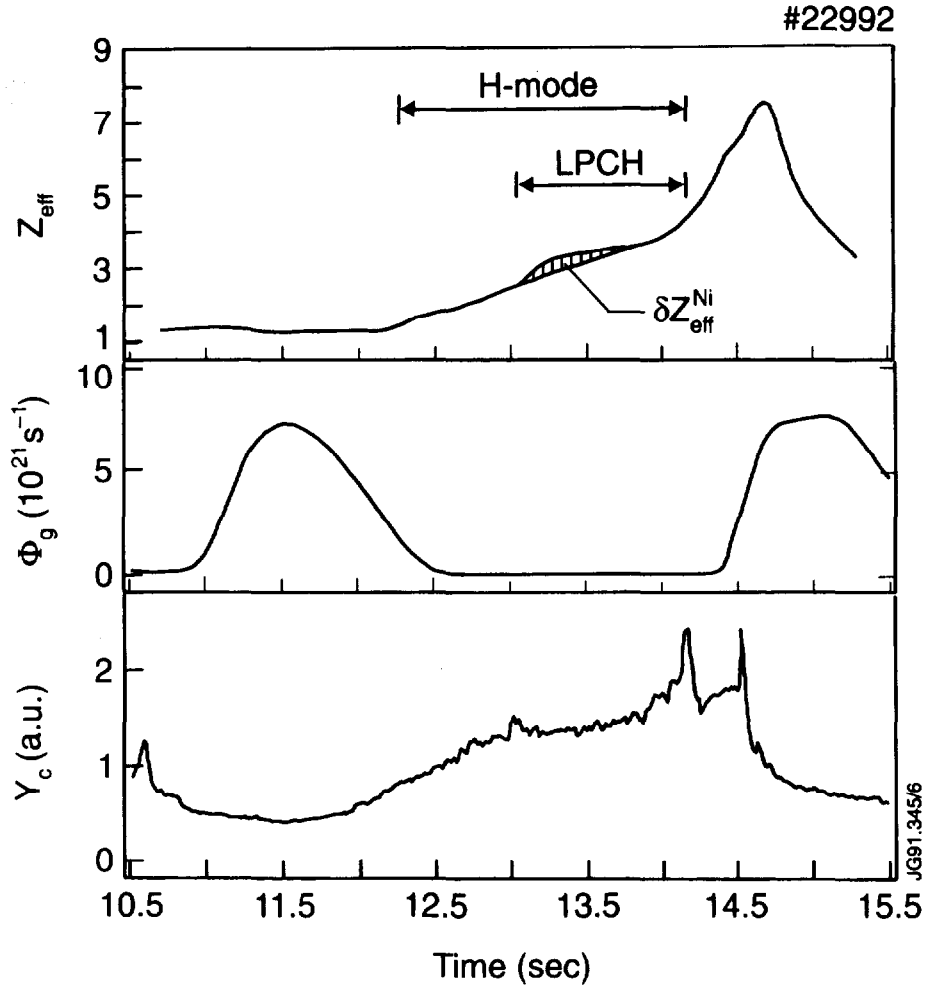

Fig.7b Z_{eff}, deuterium gas input from the valve and the approximate measure of the carbon yield(derived from the CIII and D_α light) for the same discharge as in Fig.4. The approximate contribution to Z_{eff} from the nickel injection is denoted δZ_{eff}^{Ni}.

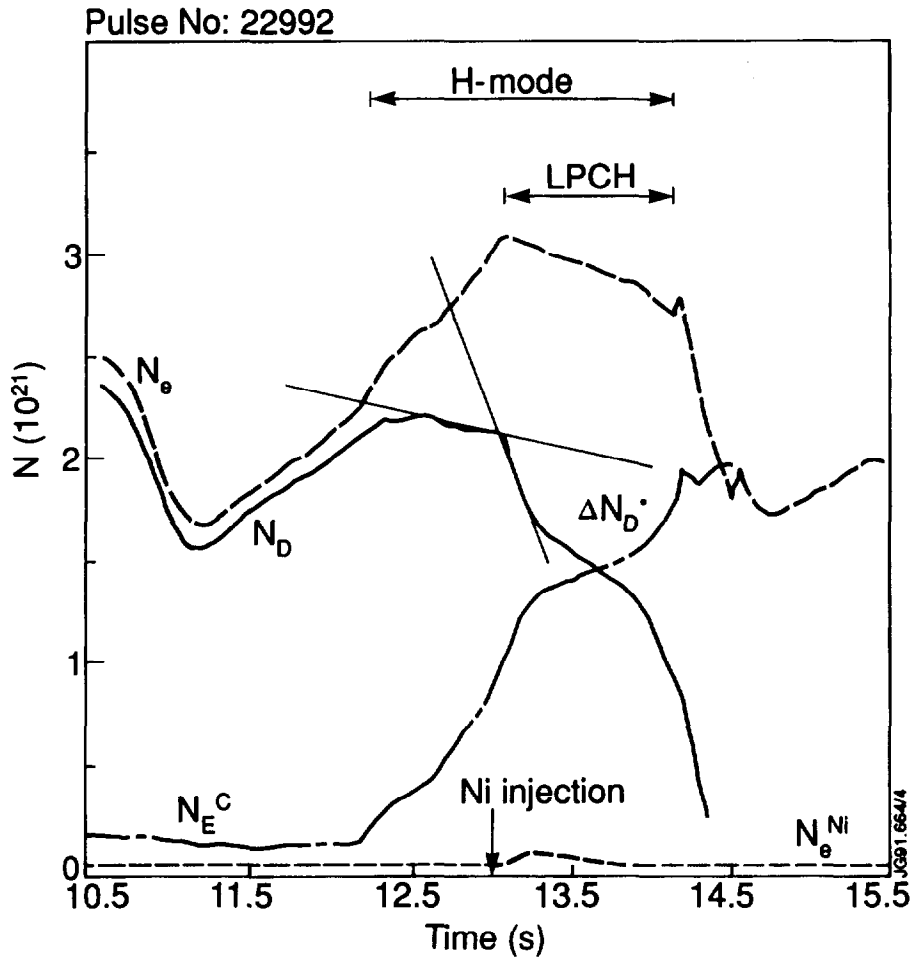

Fig.8 Evolution of the total number of electrons N_e, deuterons N_D, electrons due to carbon N_e^C and electrons due to nickel N_e^{Ni} in the plasma volume. The change of the derivatives at the H–>LPCH transition and, in particular, $\delta(\partial N_D/\partial t)$ should be noted.

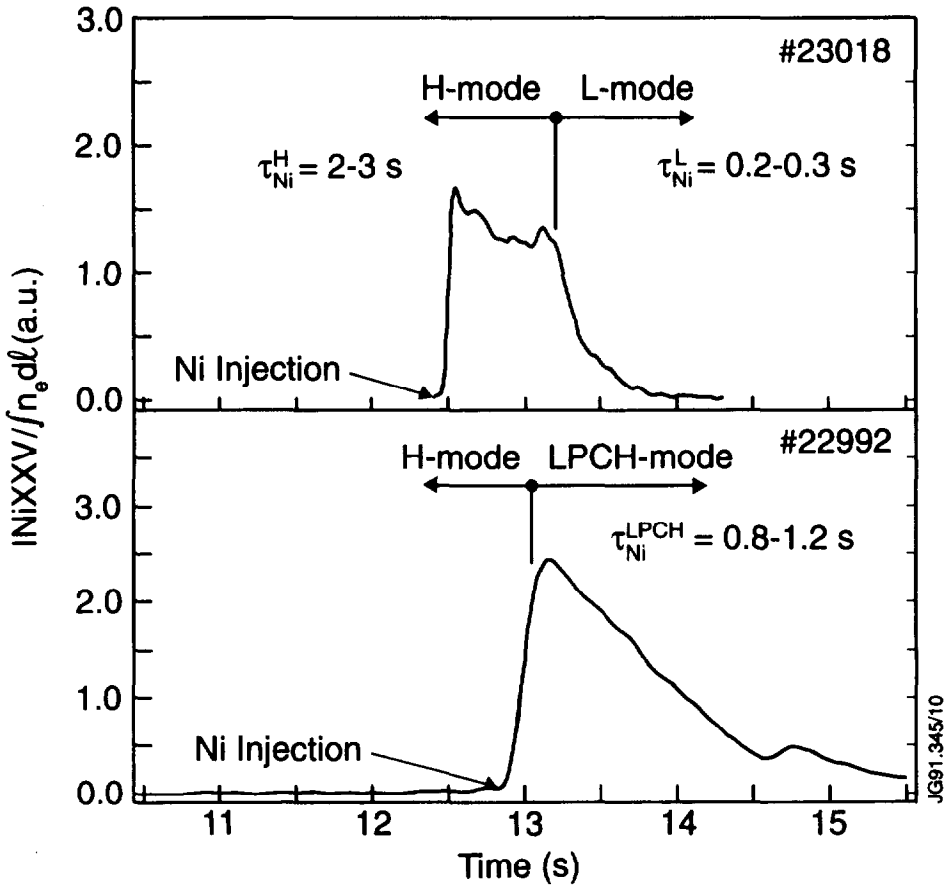

Fig.9 VUV intensity of the NiXXV line, normalised by the line average density, is plotted for 2 discharges with nickel injection. Arbitrary units in both plots are same and the signals are directly comparable. The signal of the #22992 discharge is sampled with lower sampling rate which accounts for the difference in the signal rise time.

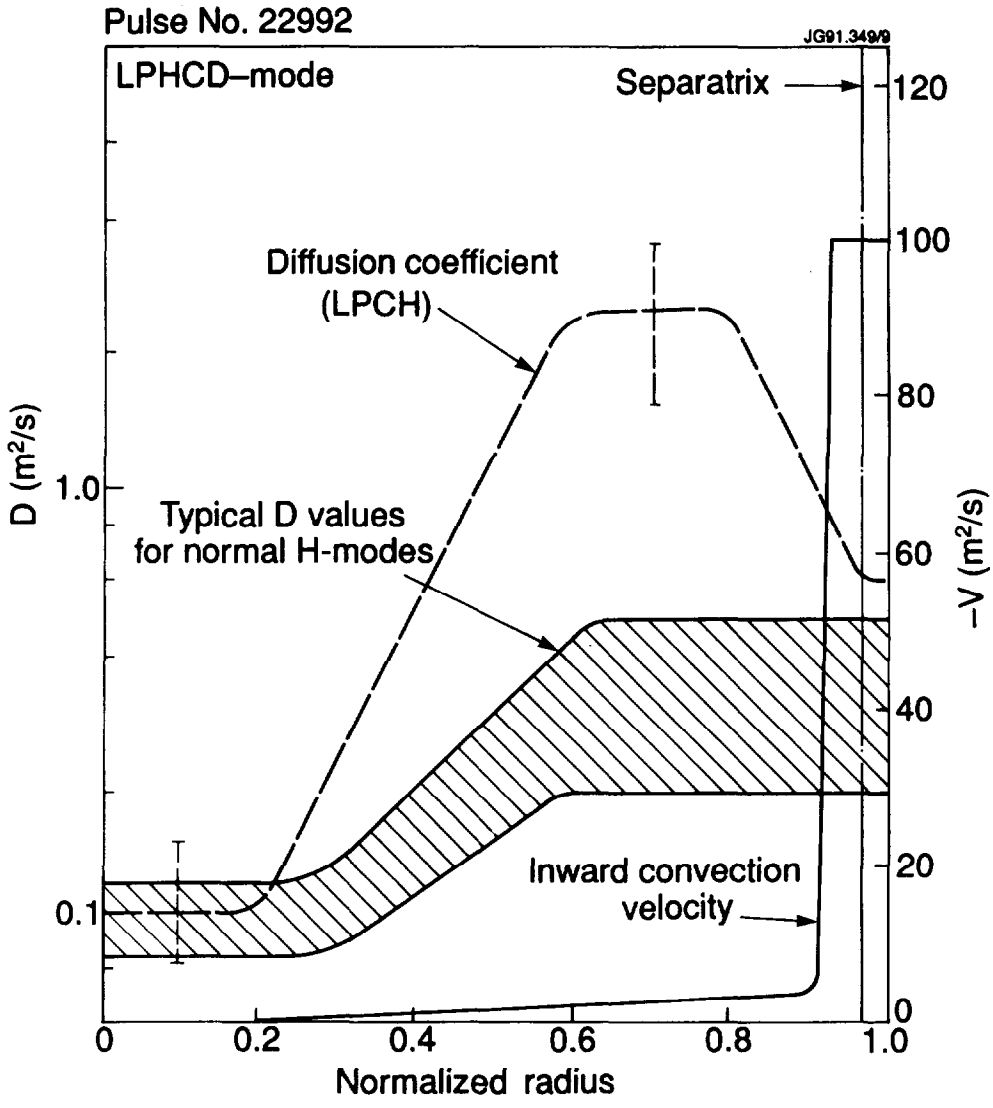

Fig.10 Radial profiles of the diffusion coefficient D(r) and the inward convection velocity V(r) plotted as a function of minor radius in the discharge #22992 derived from the evolution of the SXR–profiles and VUV intensities measured after the injection of nickel.

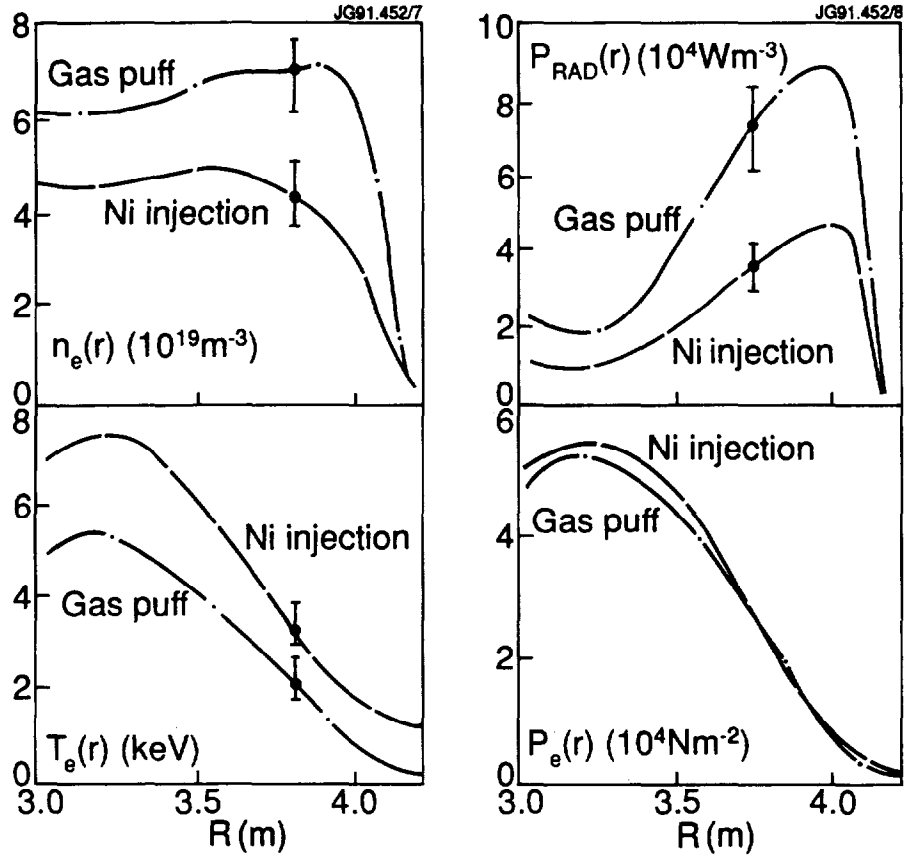

Fig.11 Radial profiles of the electron density, radiated power, electron temperature and the electron pressure during the H–>LPCH transition. The transition occured at t=13.15s following the nickel injection in the discharge #22992 and at t=13.7s in the discharge #23023 with a continuous gas puff into the x–point region. Typical error bars are ±10%.

Appendix I

THE JET TEAM

JET Joint Undertaking, Abingdon, Oxon, OX14 3EA, U.K.

J.M. Adams[1], H. Altmann, A. Andersen[14], P. Andrew[18], M. Angelone[29], S.A. Arshad, W. Bailey, P. Ballantyne, B. Balet, P. Barabaschi, R. Barnsley[2], M. Baronian, D.V. Bartlett, A.C. Bell, I. Benfatto[5], G. Benali, H. Bergsaker[11], P. Bertoldi, E. Bertolini, V. Bhatnagar, A.J. Bickley, H. Bindslev[14], T. Bonicelli, S.J. Booth, G. Bosia, M. Botman, D. Boucher, P. Boucquey, P. Breger, H. Brelen, H. Brinkschulte, T. Brown, M. Brusati, T. Budd, M. Bures, T. Businaro, P. Butcher, H. Buttgereit, C. Caldwell-Nichols, D.J. Campbell, P. Card, G. Celentano, C.D. Challis, A.V.Chankin[23], D. Chiron, J. Christiansen, C. Christodoulopoulos, P. Chuilon, R. Claesen, S. Clement, E. Clipsham, J.P. Coad, M. Comiskey[4], S. Conroy, M. Cooke, S. Cooper, J.G. Cordey, W. Core, G. Corrigan, S. Corti, A.E. Costley, G. Cottrell, M. Cox[7], P. Cripwell, H. de Blank[15], H. de Esch, L. de Kock, E. Deksnis, G.B. Denne-Hinnov, G. Deschamps, K.J. Dietz, S.L. Dmitrenko, J. Dobbing, N. Dolgetta, S.E. Dorling, P.G. Doyle, D.F. Düchs, H. Duquenoy, A. Edwards, J. Ehrenberg, A. Ekedahl, T. Elevant[11], S.K. Erents[7], L.G. Eriksson, H. Fajemirokun[12], H. Falter, D. Flory, J. Freiling[15], C. Froger, P. Froissard, K. Fullard, M. Gadeberg, A. Galetsas, D. Gambier, M. Garribba, P. Gaze, R. Giannella, A. Gibson, R.D. Gill, A. Girard, A. Gondhalekar, C. Gormezano, N.A. Gottardi, C. Gowers, B.J. Green, R. Haange, G Haas, A. Haigh, G. Hammett[6], C.J. Hancock, P.J. Harbour, N.C. Hawkes[7], P. Haynes[7], J.L. Hemmerich, T. Hender[7], F.B. Herzog, R.F. Herzog, J. Hoekzema, J. How, M. Huart, L Hughes, T.P. Hughes[4], M. Hugon, M. Huguet, A. Hwang[7], B. Ingram, M. Irving, J. Jacquinot, H. Jaeckel, J.F. Jaeger, G. Janeschitz[13], S. Jankowicz[22], O.N. Jarvis, F. Jensen, E.M. Jones, L.P.D.F. Jones, T.T.C. Jones, J-F. Junger, E. Junique, A. Kaye, B.E. Keen, M. Keilhacker, G.J. Kelly, W. Kerner, R. Konig, A. Konstantellos, M. Kovanen[20], G. Kramer[15], P. Kupschus, R. Lässer, J.R. Last, B. Laundy, L. Lauro-Taroni, K. Lawson[7], M. Lennholm, A. Loarte, R. Lobel, P. Lomas, M. Loughlin, C. Lowry, B. Macklin, G. Maddison[7], G. Magyar, W. Mandl[13], V. Marchese, F. Marcus, J. Mart, E. Martin, R. Martin-Solis[8], P. Massmann, G. McCracken[7], P. Meriguet, P. Miele, S.F. Mills, P. Millward, R. Mohanti[17], P.L. Mondino, A. Montvai[3], S. Moriyama[28], P. Morgan, H. Morsi, G. Murphy, M. Mynarends, R. Myrnäs[16], C. Nardone, F. Nave[21], G. Newbert, M. Newman, P. Nielsen, P. Noll, W. Obert, D. O'Brien, J. O'Rourke, R. Ostrom, M. Ottaviani, M. Pain, F. Paoletti, S. Papastergiou, D. Pasini, A. Peacock, N. Peacock[7], D. Pearson[12], R. Pepe de Silva, G. Perinic, C. Perry, M. Pick, R. Pitts[7], J. Plancoulaine, J-P. Poffé, F. Porcelli, L. Porte[19], R. Prentice, S. Puppin, S. Putvinsko[23], G. Radford[9], T. Raimondi, M.C. Ramos de Andrade, P-H. Rebut, R. Reichle, E. Righi, F. Rimini, D. Robinson[7], A. Rolfe, R.T. Ross, L. Rossi, R. Russ, P. Rutter, H.C. Sack, G. Sadler, G. Saibene, J.L. Salanave, G. Sanazzaro, A. Santagiustina, R. Sartori, C. Sborchia, P. Schild, M. Schmid, G. Schmidt[6], B. Schunke, S.M. Scott, A. Sibley, R. Simonini, A.C.C. Sips, P. Smeulders, R. Stankiewicz[27], M. Stamp, P. Stangeby[18], D.F. Start, C.A. Steed, D. Stork, P.E. Stott, T.E. Stringer, P. Stubberfield, D. Summers, H. Summers[19], L. Svensson, J.A. Tagle[21], A. Tanga, A. Taroni, A. Tesini, P.R. Thomas, E. Thompson, K. Thomsen, J.M. Todd, P. Trevalion, B. Tubbing, F. Tibone, E. Usselmann, H. van der Beken, G. Vlases, M. von Hellermann, T. Wade, C. Walker, R. Walton[6], D. Ward, M.L. Watkins, M.J. Watson, S. Weber[10], J. Wesson, T.J. Wijnands, J. Wilks, D. Wilson, T. Winkel, R. Wolf, B. Wolle[24], D. Wong, C. Woodward, Y. Wu[25], M. Wykes, I.D. Young, L. Zannelli, Y. Zhu[26], W. Zwingmann.

PERMANENT ADDRESSES

1. UKAEA, Harwell, Didcot, Oxon, UK.
2. University of Leicester, Leicester, UK.
3. Central Research Institute for Physics, Academy of Sciences, Budapest, Hungary.
4. University of Essex, Colchester, UK.
5. ENEA-CNR, Padova, Italy.
6. Princeton Plasma Physics Laboratory, New Jersey, USA.
7. UKAEA Culham Laboratory, Abingdon, Oxon, UK.
8. Universidad Complutense de Madrid, Spain.
9. Institute of Mathematics, University of Oxford, UK.
10. Freien Universität, Berlin, F.R.G.
11. Swedish Energy Research Commission, S-10072 Stockholm, Sweden.
12. Imperial College of Science and Technology, University of London, UK.
13. Max Planck Institut für Plasmaphysik, Garching bei München, FRG.
14. Risø National Laboratory, Denmark.
15. FOM Instituut voor Plasmafysica, 3430 Be Nieuwegein, The Netherlands.
16. University of Lund, Sweden.
17. North Carolina State University, Raleigh, NC, USA
18. Institute for Aerospace Studies, University of Toronto, Downsview, Ontario, Canada.
19. University of Strathclyde, 107 Rottenrow, Glasgow, UK.
20. Nuclear Engineering Laboratory, Lapeenranta University, Finland.
21. CIEMAT, Madrid, Spain.
22. Institute for Nuclear Studies, Otwock-Swierk, Poland.
23. Kurchatov Institute of Atomic Energy, Moscow, USSR
24. University of Heidelberg, Heidelberg, FRG.
25. Institute for Mechanics, Academia Sinica, Beijing, P.R. China.
26. Southwestern University of Physics, Leshan, P.R. China.
27. RCC Cyfronet, Otwock Swierk, Poland.
28. JAERI, Naka Fusion Research Establishment, Ibaraki, Japan.
29. ENEA, Frascati, Italy.

At 1st June 1991